NeuroImage 303 (2024) 120896

Contents lists available at ScienceDirect

NeuroImage

journal homepage: www.elsevier.com/locate/ynimg

Investigating the impact of the regularization parameter on EEG resting-state source reconstruction and functional connectivity using real and simulated data

F. Leone [a,b,*], A. Caporali [c,d], A. Pascarella [e], C. Perciballi [a,b], O. Maddaluno [a,b], A. Basti [g], P. Belardinelli [f], L. Marzetti [g,h], G. Di Lorenzo [b,i], V. Betti [a,b,*]

[a] Department of Psychology, Sapienza University of Rome, via dei Marsi 78, Rome, 00185, Italy
[b] IRCCS Fondazione Santa Lucia, via Ardeatina, 354, Rome, 00179, Italy
[c] Faculty of Veterinary Medicine, University of Teramo, via R. Balzarini 1, Teramo, 64100, Italy,
[d] International School of Advanced Studies, University of Camerino, via Gentile III Da Varano, Camerino, 62032, Italy
[e] Institute for Computational Applications, CNR, Italy
[f] CIMeC, Center for Mind/Brain Sciences, University of Trento, via delle Regole, 101, Mattarello-Trento, 38123, Italy
[g] Department of Neuroscience, Imaging and Clinical Sciences, "G. d'Annunzio" University of Chieti-Pescara, via dei Vestini, Chieti, 66100, Italy
[h] Institute for Advanced Biomedical Technologies, "G. d'Annunzio" University of Chieti-Pescara, via Luigi Polacchi, Chieti, 66100, Italy
[i] Laboratory of Psychophysiology and Cognitive Neuroscience, University of Rome Tor Vergata, Rome, Italy

ARTICLE INFO

Keywords:
EEG
Resting-state
Regularization parameter
Source reconstruction
Minimum Norm Estimation
Functional connectivity

ABSTRACT

Accurate EEG source localization is crucial for mapping resting-state network dynamics and it plays a key role in estimating source-level functional connectivity. However, EEG source estimation techniques encounter numerous methodological challenges, with a key one being the selection of the regularization parameter in minimum norm estimation. This choice is particularly intricate because the optimal amount of regularization for EEG source estimation may not align with the requirements of EEG connectivity analysis, highlighting a nuanced trade-off. In this study, we employed a methodological approach to determine the optimal regularization coefficient that yields the most effective reconstruction outcomes across all simulations involving varying signal-to-noise ratios for synthetic EEG signals. To this aim, we considered three resting state networks: the Motor Network, the Visual Network, and the Dorsal Attention Network. The performance was assessed using three metrics, at different regularization parameters: the Region Localization Error, source extension, and source fragmentation. The results were validated using real functional connectivity data. We show that the best estimate of functional connectivity is obtained using 10^{-2}, while 10^{-1} has to be preferred when source localization only is at target.

1. Introduction

Spontaneous brain activity, *i.e.*, without any external stimulus or task, is far from random noise. Rather, it is temporally and spatially organized into coherent regions of similar functionality that resemble those observed during the execution of cognitive, motor, and visual tasks (Smith et al., 2009). Most studies have used functional magnetic resonance imaging (fMRI) to measure temporal correlation (functional connectivity - FC) between blood- oxygenation-level-dependent (BOLD) signals from different brain areas. These studies identified several resting-state networks (RSNs), highly reproducible across subjects (Biswal et al., 1995; Raichle et al., 2001; Fox et al., 2005). However, fMRI has a low temporal resolution. Moreover, the BOLD signal is only an indirect measure of the neural sources related to hemodynamics. Non-invasive electrophysiological imaging techniques, *i.e.*, electroencephalography (EEG) and magnetoencephalography (MEG), have an excellent temporal resolution on the scale of milliseconds. Using MEG (de Pasquale et al., 2010, 2012; Brookes et al., 2011; Hipp et al., 2012; Marzetti et al., 2013; Betti et al., 2013; V. 2018) and high-density EEG (Siems et al., 2016; Sockeel et al., 2016; Knyazev et al., 2016; Liu et al., 2017; Q. 2018) similar RSNs were uncovered.

Researchers investigated connectivity in source space rather than

* Corresponding authors.
E-mail addresses: f.leone@uniroma1.it (F. Leone), vi-viana.betti@uniroma1.it (V. Betti).

https://doi.org/10.1016/j.neuroimage.2024.120896
Received 15 May 2024; Received in revised form 4 October 2024; Accepted 18 October 2024
Available online 8 November 2024

sensor space to address inaccuracies and ambiguities stemming from volume conduction spread. This type of analysis can help mitigate these issues (Schoffelen and Gross, 2009). This analysis strategy implies estimating the underlying current sources, a commonly encountered ill-posed problem where numerous source configurations can equally account for the data. Moreover, the inverse problem is not continuously dependent on the data due to small perturbations from noise leading to large variations in the solution (Grech et al., 2008). Using a regularization method is a classic mathematical approach to address the ill-posed nature of inverse problems, as it reintroduces solution uniqueness by incorporating prior information (Hanke and Hansen, 1993; Baillet et al., 2001; Grech et al., 2008; Sorrentino and Piana, 2017; Ilmoniemi and Sarvas, 2019). Different a-priori information/constraints depend on different inverse methods, yielding diverse source estimates. Minimum Norm Estimation (MNE) is a widely used method in which the solution is obtained by looking for a source distribution with minimum energy that best fits the data (Lin et al., 2004; Ramírez et al., 2011). The regularization parameter λ that tunes the balance between the solution accuracy and its numerical stability can be determined by using an inversely proportional relationship with the Signal-To-Noise Ratio (SNR) (Lin et al., 2004; Ramírez et al., 2011). In task-evoked studies, the typically defined SNR value is set to 3 (Baillet et al., 2001). However, this value, a default parameter in Brainstorm (Tadel et al., 2011) and MNE-python (Gramfort et al., 2013), is not necessarily suited for studying the connectivity at rest.

The optimal selection of the regularization parameter is still debated, with increasing interest in studying its impact on functional connectivity (Vallarino et al., 2021, 2023). Moreover, most existing studies employed MEG and there remains a lack of methodological EEG investigations in this domain. In this technical note, we aim at determining the optimal λ value for source-space connectivity detection at rest in a minimum-norm source estimation setting with a realistic head model.

To do so, we simulated synthetic resting-state EEG signals with different known SNRs. Three different metrics were introduced to evaluate the solution of the inverse problem: i) the region localization error, ii) the spatial dispersion, and iii) the source fragmentation. Finally, the source reconstruction results were employed for real data functional connectivity estimation. The ultimate goal of this work is to obtain an optimal regularization parameter based on quantitative metrics that encompass several key factors for source and functional connectivity estimations. With respect to the state of the art, determining the appropriate values for these parameters is not straightforward. For this reason, our study aims to introduce a standardized protocol to ensure the reproducibility of both the simulated and real data results. Additionally, a proper evaluation of source estimation techniques is necessary to use functional connectivity as a reliable research tool and mitigate the subjectivity involved in the analysis process.

2. Materials and methods

2.1. Generation of synthetic EEG signal in resting-state networks

The head and sensor models used to generate the EEG signal were based on the New York Head model[1] (Huang et al., 2016). It contains: i) a segmentation of the ICBM-152 template head (De Leener et al., 2018) into six different tissue types (*i.e.* skin, skull, cerebrospinal fluid, grey matter, white matter, and air cavities); ii) a triangulated cortical mesh with 74.382 vertices; iii) labels and locations of 231 EEG scalp electrodes defined in accordance with the 10–5 electrode system.

We computed a three-layer boundary-element method (BEM) (Oosten- dorp and Van Oosterom, 1989) volume conductor model of the head based on the geometry and the electrical propriety of the New York Head, considering the following conductivity values: 0.3, 0.004 and 0.3 S/m for brain, skull, and scalp, respectively. We then used a uniform subsample of 10.016 nodes of the New York Head cortical mesh for the source space. Finally, we considered 228 electrodes out of 231 (3 electrodes around the base of the neck were removed) as sensor space. Using these models, we computed the lead-field matrix L, with source orientations normal to the local cortical surface, using the Dipoli BEM method integrated into the Fieldtrip toolbox (Oostenveld et al., 2011). This matrix was used for the generation of the EEG signal, as in (Basti et al., 2022).

Specific generation parameters were selected for the EEG data simulation, including source position (refer to Table 1), adjacency matrix, time delay, sampling frequency, length of time series, frequency band, number of brain noise point-like sources, and SNR, divided into signal-to-brain-noise ratio

(SBNR) and signal-to-sensor-noise ratio (SSNR). The locations of the simulated sources were set to that of the nodes of three different RSNs, which were considered for their functional and clinical relevance: the Motor Network (MN), which provides information about motor control and motor task activities; the Visual Network (VIS) about visual perception; and the Dorsal Attention Network (DAN) about the spatial attention. It has been shown that there is a hierarchical functional organization between RSNs (Doucet et al., 2011; Fox et al., 2005). This hierarchy can be found in the selected RSNs, since the VIS is representative of the lowest functional level, the MN of a higher level than VIS, and the DAN can be considered the highest functional level. Every point-like source within each considered RSN was coupled to one another source belonging to the same RSN. Each network was simulated separately from the others. Source locations for the different nodes in each RSN are listed in Table 1.

For each RSN, the simulated EEG signal was 1 min long and sampled at 256 Hz. It was generated from synthetic source time courses, using non-linear dipolar coupled sources and 50 uncorrelated noise sources, randomly distributed over the whole cortex. SBNR ranged as [10 20 50 100], while SSNR as [1 5 10 15 20 30 40 50 75 100]. We performed 10 simulations for each RSN: in each simulation, one of the different values of SSNR was considered.

The ground truth signal was simulated as a summation of sinusoids with random amplitudes ranging from 0 to 1. The frequencies ranged between 8 and 15 Hz (alpha band), with a step of 0.01 Hz, and the phase delay was randomly chosen between 0 and 2π, uniformly distributed. These signals were then processed using an autoregressive model of order 5 to introduce temporal dependencies within each source's time series, without imposing dependencies between sources (A. Basti et al., 2018; Sommariva et al., 2017; Haufe et al., 2013; Chella et al., 2019). We subsequently modeled amplitude interactions between sources. In each direct coupling, the amplitude of the following source was a delayed version of the amplitude of the leading source, with a delay of 15 ms, while the phase of the signal in the following source was preserved. This approach ensured that the influence of the leading source manifested only through amplitude modulation, without altering the phase independence between the sources. If the adjacency matrix contained indirect paths between sources, the time delay was adjusted for the associated connections. Specifically, the delay from one source to another was increased to account for the influence of an intermediate source, and redundant direct connections were eliminated. This process reduced the complexity of the network while preserving the essential (direct and directional) amplitude dynamics. A normally distributed noise with an amplitude equal to the 2 % of the amplitude of each source was added to take into account noise from interacting sources. This signal was then multiplied by the columns of the lead field matrix corresponding to the selected source locations to account for the volume conduction from sources to sensors.

The EEG signal was modeled as a summation of the ground truth signal and of a mixture of independent standard normal processes distributed both over randomly chosen cortical nodes and electrodes. This approach aims to model the presence of both biological noise and

[1] Available on www.parralab.org/nyhead.

Table 1
Considered source positions divided into RSNs (Smith et al., 2013).

Motor Network				Dorsal Attention Network				Visual Network			
Nodes	MNI Coordinates (mm)			Nodes	MNI Coordinates (mm)			Nodes	MNI Coordinates (mm)		
vPoCe	57.95	−16.22	37.74	FEF	25.44	−5.36	53.40	V7-POSd	−5.08	−85.39	40.61
dPrCe	25.81	−12.80	58.56	FEF	−22.85	−1.46	57.91	V3-V3A	9.52	−89.44	34.40
SMA	10.80	−34.39	50.33	vIPS	−30.27	−77.82	21.64	LO	−37.15	−90.14	13.81
mdSPL	9.53	−39.92	56.83	vIPS	34.11	−79.02	24.00	Fovea-LO	−24.49	−96.37	2.62
vPoCe	−59.74	−19.10	39.65	mt	−44.04	−61.23	−0.45	LOMT	44.37	−76.41	−12.00
dPrCe1	−23.16	−14.71	74.61	mt	48.60	−61.98	−2.57	V3A	29.33	−87.72	28.83
SMA2	−11.90	−15.93	41.15	aIPS	−31.04	−37.38	46.96				
dmSP2	−5.17	−41.50	58.62	pIPS-SPL	−10.89	−63.63	53.23				
M1	−40.89	−18.73	69.11	pIPS-SPL	21.67	−65.40	47.40				
M1	40.89	−18.73	69.11	dPoCe	−44.41	−34.61	46.75				
				dPoCe	51.17	−27.64	52.69				
				PrCe	−46.66	1.07	33.49				
				PrCe	46.66	1.07	33.49				
				IFG	43.19	38.28	6.56				

instrumental noise, according to the following model:

$$x(t) = x_i(t) + x_b(t) + x_n(t) \tag{1}$$

where x_i is the previously described ground truth signal component generated by the interacting sources,

$$x_b(t) = \gamma_1 \sum_{j=1}^{50} l_j s_j^{noise}(t) \tag{2}$$

is the biological noise from 50 uncorrelated sources randomly distributed over the entire cortex, and

$$x_n(t) = \gamma_2 \cdot \mathbf{n}(t) \tag{3}$$

represents sensor noise. In Eqs. (2) and (3), $\mathbf{l_j}$ represents the column of the lead field matrix corresponding to the j-th noise source; $\mathbf{n}(t)$ is, instead, the unweighted vector of sensor noise. Finally, γ_1 and γ_2 represent scaling parameters that respectively determine the influence of biological noise and sensor noise, defined as follows: γ_1 is the ratio between the maximum variance of the true signal and the maximum variance of the noise from non-interacting sources, multiplied by the amount of added noise indicated by SBNR. Similarly, γ_2 was computed using the variance of the noise from non-interacting sources instead of interacting sources, multiplied by SSNR.

Following the previous approach, we also performed additional simulations by modeling fully connected networks (*i.e.*, networks where nodes were all connected to each other) and fully unconnected networks, where nodes were all independent among them. We then computed the difference between the ground truth FC and the FC reconstructed with different regularization parameter values for both types of networks.

2.2. Source reconstruction and performance evaluation

We performed an independent component analysis (ICA) via the fastICA algorithm (Hyvarinen, 1999) on the EEG simulated signals. Then, we solved the inverse problem for the sensor-level maps of the different Independent Components (ICs). To maintain consistency with the pipeline employed for real EEG data, we computed again the lead field matrix using the New York Head BEM volume conductor model for 228 electrodes. Using the same models to solve both the forward and the inverse problem may lead to the so-called "inverse crime" (Kaipio and Somersalo, 2007): nevertheless, the bias from the inverse crime was even on all the λ values, and it did not influence our trend results. We checked this by solving the inverse crime on a subsample of 7.564 nodes from the New York Head cortical mesh: these nodes were completely distinct from the 10.016 nodes used in EEG signal generation. The results from this inverse crime check are provided in SI in Fig. A.3.

The inverse problem was solved using Tikhonov-regularized Minimum Norm Estimation (MNE) approach. The objective of Tikhonov (*i.e.* MNE) regularization is to achieve an estimation of distributed source activity that finds a balance between minimizing the overall source amplitude, accurately reconstructing measured signals, and effectively rejecting noise (Hämäläinen et al., 1993). This means that the MNE solution is found as

$$\widehat{x}_\lambda = argmin_x \left|\left|Lx - y\right|\right|^2 + \lambda \left|\left|x\right|\right|^2 \tag{4}$$

The MNE solution is strongly dependent on the regularization parameter λ; its value is typically based on the SNR value, as in the following equation (Dale et al., 2000; Lin et al., 2004):

$$\lambda = \frac{tr(LRL^T)}{tr(C) * SNR^2} \tag{5}$$

where L is the lead field matrix, and C and R stand for noise covariance and source covariance, respectively. If prewhitening is applied to EEG data, C is reduced to identity matrix I and then $\lambda = \frac{1}{SNR^2}$. This value of SNR can be chosen independently from the real SNR of the data (which is usually impossible to know), and the most widely used value in this application is 3.

Four different performance metrics were evaluated in this study: the Region Localization Error (RLE), the Spatial Dispersion (SD), the Overall Amplitude (OA), and the number of clusters obtained with the Density-Based Spatial Clustering of Applications with Noise (DBSCAN) algorithm (Ester et al., 1996). These metrics were evaluated by varying 30 different λ values, spanning from 10^{-4} to 10^2. These values for λ were computed using Eq. (5), with the following set of SNR values: 0.1, 0.5, 1, 2, 3, 4, 5, 6, 7, 8, 9, 10, 11, 12, 13, 14, 15, 16, 17, 18, 19, 20, 30, 40, 50, 60, 70, 80, 90, and 100.

Region Localization Error (Yao and Dewald, 2005) was introduced to quantify localization accuracy, and it is defined in Eq. (6), where Q represents the number of simulated sources, $\widehat{Q}$ represents the estimated active sources (computed as the number of cortical points where the solution exceeds the 80 % of its range), s_j is the position of the actual sources and d_i is the position of the estimated sources. The first component of Eq. (6) evaluates the average distance from each estimated source to the closest real source. The remaining real sources, which are not identified, form the elements of set J. In the subsequent component of the equation, the average distance is calculated between each undetected source and its nearest estimated source. The expected value for RLE (in the ideal case) is zero, if not the lowest possible.

$$RLE = \frac{1}{Q}\sum_{i}^{Q} min_j \|d_i - s_j\| + \frac{1}{\widehat{Q}}\sum_{j\in J}^{\widehat{Q}} min_i \parallel \; s_j - d_i \; \parallel \tag{6}$$

To quantify spatial extension, Spatial Dispersion (Molins et al., 2008;

Hauk et al., 2011; Todaro et al. 2019) was used: it is a measure of the "width" of the distribution around the cortical map peak, and it is defined as in Eq. (7) where N is the number of cortical points, D_j stands for the distance between the peak of the solution and the j-th cortical point, F_j stands for the value of the reconstructed current in the j-th point. In an ideal case, the expected value for SD is the lowest possible: it cannot be zero either in ideal case, because the MNE algorithm finds a distributed solution, therefore it will never find a solution which comprises only a single source point.

$$SD = \sqrt{\frac{\sum_{j=1}^{N} D_j F_j^2}{\sum_{j=1}^{N} F_j^2}} \tag{7}$$

Overall Amplitude (Hauk et al., 2011), defined as in Eq. (8), was also considered. This metric is used to take into account the different depths of source points; nevertheless, this study does not focus on the evaluation of deep sources reconstruction due to the intrinsic limits of the unweighted MNE algorithm. In fact, it emphasizes lower amplitude superficial sources with respect to higher amplitude deep sources, and this makes it unsuitable to study deep sources. We include this metric anyway for the sake of completeness in Eq. (8), but we do not have an expected optimal value for this metric.

$$OA = \frac{\sum_{j=1}^{N} |F_j|}{max_j |F_j|} \tag{8}$$

Finally, the number of clusters was introduced as a metric to evaluate the source fragmentation, by using the DBSCAN algorithm: this method (Ester et al., 1996) was designed to cluster data of arbitrary shapes in the presence of noise in spatial and non-spatial high dimensional databases. We chose it over the k-means algorithm (Ahmed et al., 2020) for its ability to identify clusters of non-circular shape and because it does not need the number of clusters as an input parameter. It needs two hyper-parameters: the minimum number of points (*MinP*) clustered together for a region to be considered dense and a distance (ε) measure that will be used to locate the points in the neighborhood of any given point. In this work, we chose $MinP = 2$ and $\varepsilon = 8$ mm. To apply the algorithm, we selected a region of interest (ROI) in every IC topography: the ROI was defined as the source space points where the inverse solution was over 60 % of the range of the solution over the whole brain. The DBSCAN algorithm was applied providing the coordinates of the source points in the ROI. To determine which λ value provided the best reconstruction, we focused exclusively on source maps reconstructed from IC showing a clear dipolar pattern (identified by visual inspection), ensuring that the optimal number of clusters was always 1.

2.3. EEG signal data collection

2.3.1. Participants

EEG signal was recorded from 31 healthy participants (17 men, 14 women; mean age ± sd = 26.7 ± 4.1 years old). Informed consent was obtained from all the participants. The experimental protocol was approved by the local ethical committee at the Santa Lucia Foundation IRCCS (Prot. CE/PROG. 717) and was conducted according to the ethical standards of the Declaration of Helsinki.

2.3.2. Data collection

A 10-minute resting-state EEG signal was recorded with a 256-electrode ANT EEG system (ANT Neuro, The Netherlands), using a waveguard™ original EEG cap with 256 channels located following an equidistant hexagonal layout. The ground electrode was placed on the left mastoid, and the reference electrode at the Z12Z channel, which is located over the centroparietal scalp middle line of the interhemispheric fissure. Peripheral data, such as electrocardiographic (ECG) and electrooculographic signal (vertical and hor- izontal - VEOG/EOG) were acquired to be used in the cleaning phase of the EEG signal from artifact contamination. We used two EOG channels (one for vertical eye movements and one for horizontal movements) and two ECG channels, which were placed under participants' clavicle. EEG data were recorded with a sampling rate of 2048 Hz. Data were collected while participants were comfortably seated fixating a small black cross on a white background without any other sensory, motor or cognitive task to perform.

2.3.3. EEG preprocessing and source reconstruction

EEG preprocessing was carried out using Fieldtrip (Oostenveld et al., 2011). First, raw data were down-sampled at 256 Hz and band-passed filtered within the 1–102 Hz frequency range. Outlier channels and signal epochs were automatically identified and removed from further analysis. Specifically, noisy channels were identified by assessing the following metrics: i) the low signal similarity, estimated by computing the correlation between each channel and its neighbors. We used a correlation threshold equal to 0.6. In addition, a bad channel is identified by searching for outliers in the neighbor correlation distribution setting a statistical threshold (equal to 2.5 standard deviations below the mean neighbor correlation from all the channels). Another additional criterion was the ratio between the standard deviations of each channel and its neighbors (Winter et al., 2007): a bad channel is identified if its standard deviation is more than 50 % higher than that of its neighbors (thus our variance ratio threshold is equal to 0.5); ii) the deviation from the distribution of channel weights obtained by an ICA-based approach (fast-ICA algorithm). Epochs containing large bursts of high-frequency activity were detected and removed. Then we used an ICA approach to classify components as brain-generated or artifact according to different parameters: 1) correlation of the IC time course with those of EOG/VEOG and ECG reference channels: 2) correlation of the IC Power-Spectral Density (PSD) with those of EOG/VEOG and ECG reference channels; 3) correlation of the IC Power Time-Course with those of EOG/VEOG and ECG channels; 4) kurtosis; 5) 1/f trend of PSD; 6) flat- ness of PSD. ICs were band-passed (1–102 Hz) and notch-filtered (49–51/99–101 Hz). If only one parameter did not reach the threshold, the component was classified as an artifact. This analysis pipeline was adapted from the MEG preprocessing pipeline (Larson-Prior et al., 2013) used by the Human Connectome Project, as in our previous study (Maddaluno et al., 2024).

Source estimation for real data was carried out with the same pipeline described for the artificial signal, except for two steps: i) the volumetric segmentation and cortical reconstruction were performed with the Freesurfer image analysis suite using individual MRIs data of each participant; ii) the cortical mesh is composed by 8004 vertices instead of 10,016 points of the New York Head.

2.4. Estimation of BLP functional connectivity

Functional connectivity was estimated for both simulated and real data. For the simulated data, FC was calculated separately for each of the three considered RSNs, focusing solely on connectivity within each RSN. For the real data, our analysis was focused on a subset of the original 8004 vertices, which included nodes with functional importance. In detail, we examined a parcellation scheme composed of 164 vertices of the source space belonging to 10 RSNs: Auditory Network (AN); Control Network (CN); Dorsal Attention Network (DAN); Default Mode Network (DMN); Fronto-Parietal Network (FPN); Language Network (LN); Motor Network (MN); Ventral Attention Network (VAN); Visual Foveal Network (VFN); Visual Peripherical Network(VPN). Specific MNI coordinates are associated with each vertex, as reported in previous studies (Baldassarre et al., 2014; de Pasquale et al., 2021).

Before estimating the functional connectivity, we applied the Geometric Correction Scheme (GCS), as in (Wens et al., 2015; V. Betti et al., 2018). We subsequently determined the Band Limited Power (BLP) (de Pasquale et al., 2010, 2012) temporal patterns from the source space signals in α (8–15 Hz), low β (15–26 Hz) and high β (26–35 Hz) frequency bands as the average of the squared activity magnitude within a

400-millisecond sliding window, sampled at a rate of 50 Hz. Considering a couple of nodes i and j, the static functional connectivity can be defined as follows Eq. (9):

$$FC = \left\{ \frac{corr(BLP(i), BLP(j)_{\perp i}) + corr\left(BLP(j), BLP(i)_{\perp j}\right)}{2} \right\}, if\ d(i,j) > 1.5;\ NaN,\ otherwise \quad (9)$$

where corr(x,y) is the Pearson's correlation coefficient between signals x and y, $BLP\ (i)_{\perp j}$ is the BLP computed on the time series of node i in which the GCS was applied with respect to node j (see details in (Wens et al., 2015; V. Betti et al., 2018)), d(i,j) is the Euclidean distance between nodes i and j, and NaN is a "not a number" element for masking correlation coefficients between nodes closer than 15 mm.

BLP FC on simulated data was computed using both the ground truth signal x_i and the reconstructed signal with varying regularization parameters. We then calculated the relative error for both the fully connected and fully unconnected simulations to assess whether the choice of regularization parameter could introduce a bias in the over- or underestimation of FC.

On the other hand, to describe the difference between FC with different λ values in real data where we did not have a ground truth value, we computed the percentage relative difference, defined in Eq. (10), where $FC_{\lambda=10^{-x}}$ represents the functional connectivity estimated with different regularization parameters.

$$\Delta FC_{\%} = \frac{FC_{\lambda=10^{-2}} - FC_{\lambda=10^{-1}}}{FC_{\lambda=10^{-2}}} \quad (10)$$

2.5. Statistical analyses

To analyze the differences between RLE, OA and SD distributions, we ran a one-way ANOVA ($\alpha = 0.05$) with 4 factors, represented by λ interest values. Then, we carried out the Bonferroni correction post-hoc test. Percentage of occurrence distributions derived from DBSCAN clustering were compared using multiple two sample chi-squared tests ($p < 0.05$). Simulated FC differences between ground truth FC and reconstructed FC were tested with a paired *t*-test (two tails). Regarding real-data functional connectivity differences we ran repeated measures ANOVA ($\alpha = 0.05$), with Bonferroni correction for post-hoc multiple comparisons with band (α, low β, high β), λ (equals to 10^{-1} and 10^{-2}), and resting state networks (DAN, VIS, MN) as within-subject factors averaged across connections of the three defined RSNs.

3. Results

3.1. Source reconstruction

First, we applied the analysis pipeline outlined in Fig. 1 above to the synthetic EEG signals, generated using the procedures outlined in "Materials and methods" Section. Then, we examined the effects of the optimum λ value on the functional connectivity analysis in real EEG data.

Fig. 2 presents the trends (in a semi-logarithmic scale) of the three metrics, averaged across all components obtained for all simulations, introduced in Section 2.1, to assess the performance of the source reconstruction. In detail, Fig. 2A shows the RLE metric, which decreases as λ increases. Fig. 2B shows the SD metric: this increases as the λ increases, meaning that the reconstructed sources become more spread as λ increases. At last, Fig. 2C shows the OA metric: this increases when λ increases, similarly to SD.

For all three metrics, the λ values of major interest are presented as bullet points in Fig. 2: the 10^{-4} and 10^{2} values appear to be the extreme points of the distribution of the metrics, while the value 10^{-1} has been chosen as it is traditionally used in many EEG analysis pipelines (Calvetti et al., 2019). Moreover, the λ value equal to 10^{-2} appears to be another notable point from methodological MEG literature (Vallarino et al., 2021, 2023), which indicates that the optimal regularization parameter for connectivity estimation must be at least an order of magnitude lower than the one used for source localization.

Prior to the full analysis, we present a visual representation of the changes occurring in source reconstruction when varying the λ values (Fig. 3): this figure showcases an example of IC topographies for the RSNs of interest. The visualizations reveal a clear trend in the enlargement of reconstructed source sizes with increasing λ. Additionally, we observe shifts in the peak of the solution as λ varies, and a corresponding fragmentation of sources at lower λ values.

Next, we focused on the analysis of the SD, OA, and RLE metrics for only the four points of interest of λ (10^{-4}, 10^{-2}, 10^{-1}, 10^{2}), as reported

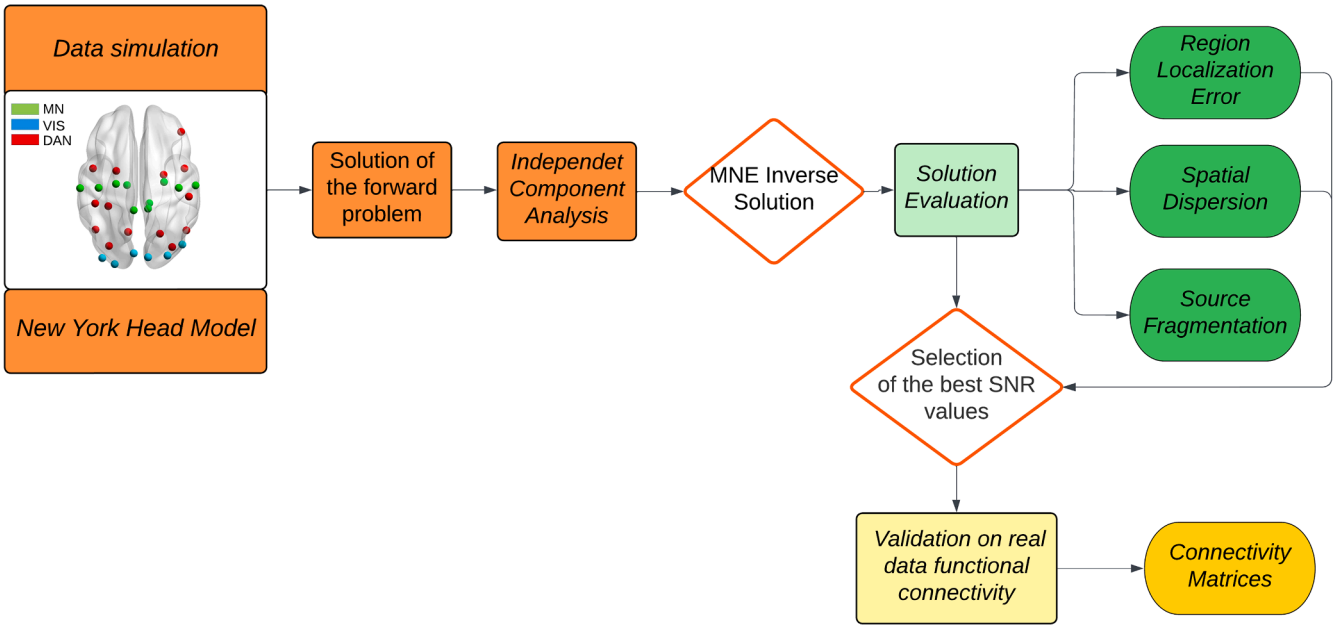

Fig. 1. The analysis pipeline of this study is structured in a data simulation step (orange), the introduction of three metrics to analyze simulated data (green), and their validation on real data (yellow).

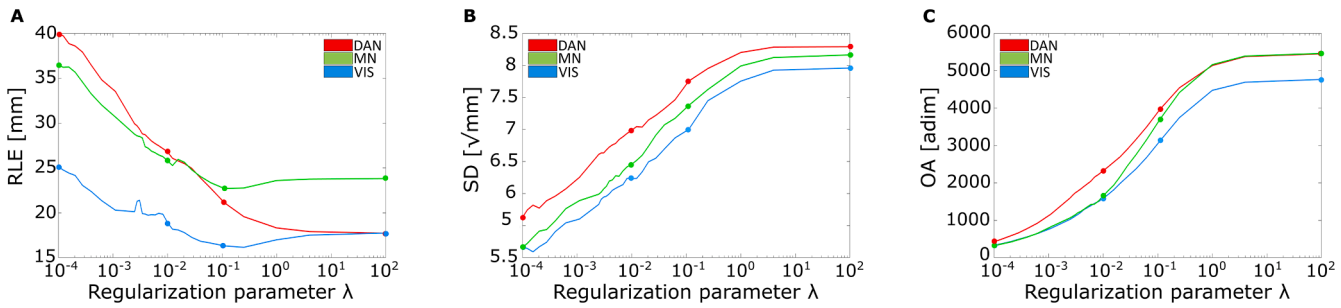

Fig. 2. A. Region Localization Error (RLE) 2.B. Spatial Dispersion (SD) and 2.C. Overall Amplitude (OA) trends computed in 30 λ values spanning from 10^{-4} to 10^{2}. Visual Network (VIS) results are given in cyan; Motor Network (MN) in green; Dorsal Attention Network (DAN) in red. The bullet points indicate the λ values of interest 10^{-4}, 10^{-2}, 10^{-1}, and 10^{2}.

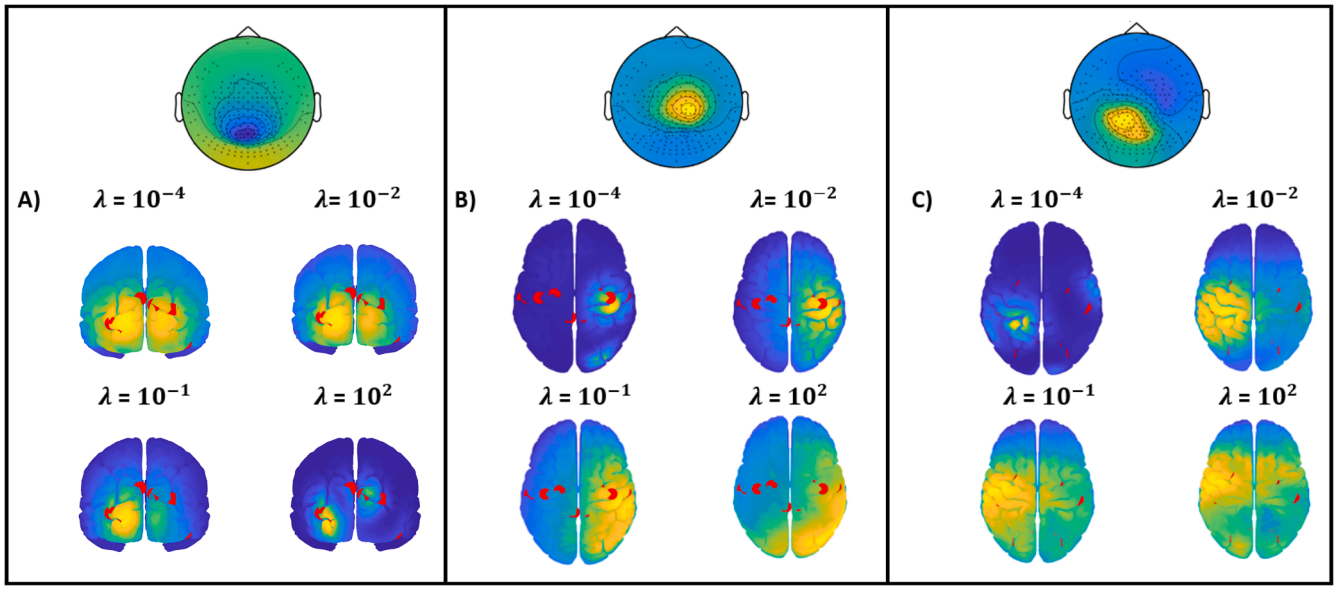

Fig. 3. Example of IC topographies at λ values of interest (10^{-4}, 10^{-2}, 10^{-1}, and 10^{2}); A) Visual Network (VIS) component; B) Motor Network (MN) component; C) Dorsal Attention Network (DAN) component. Red points represent ground truth positions of the simulated sources.

in Fig. 4. The red box plots represent the RLE, OA and SD for the DAN network: specifically, for the RLE metric, we found a statically significant difference between 10^{2} and 10^{-2}, and between 10^{-2} and 10^{-4} ($F_{3,228} = 81.36$, $p < 0.05$). The OA ($F_{3,210} = 486.67$, $p < 0.05$) and SD ($F_{3,138} = 102.15$, $p < 0.05$) metrics present a significant difference for every λ distribution. For the MN, the green box plots show the results for the three metrics: for the RLE, there was a statistically significant difference between 10^{2} and 10^{-4} values ($F_{3,165} = 9.38$, $p < 0.05$). Also for this network, the OA ($F_{3,129} = 260.20$, $p < 0.05$) and SD ($F_{3,93} = 56.50$, $p < 0.05$) metrics present a significant difference for every λ distribution. Finally, for the VIS (the cyan box plots), no significant differences in the RLE metric were found across the λ distribution. Conversely, for the SD ($F_{3,117} = 63.42$, $p < 0.05$) and OA ($F_{3,183} = 354.16$, $p < 0.05$) metrics presented statistically significant differences between every λ value. Similar results were observed for the real data, which are presented in SI in Fig. A.1.

To evaluate the performance of the source reconstruction, in terms of the fragmentation of the MNE solution, we introduced the cluster analysis that reduced dimensionality data into groups using the DBSCAN algorithm. In Fig. 5, it is reported an example of the clustering results (C) for a selected IC, for different λ values compared with the reconstructed topography (B) and the sensor level map (A). Fig. 6 reports the percentage of occurrences of clusters in real data: it shows that the percentage of true detections of only one cluster is significantly higher when λ is 10^{-1}, as compared to 10^{-4}, 10^{-2} and 10^{2} ($\chi^2_{(9)}$=44.68, $p <$ 0.001; $\chi^2_{(8)}$= 38.40, $p < 0.001$; $\chi^2_{(6)}$= 17.14, $p = 0.009$, respectively). We can notice that the highest fragmentation is found when λ is 10^{-4} and 10^{-2}, with no statistically significant difference between them. This high fragmentation is expected, as minimal regularization leads to reduced numerical stability in the solution, as in Eq. (4). On the other hand, fragmentation is reduced for $\lambda = 10^{2}$ due to strong regularization, which tends to diffuse the solution across the brain, as observed in the SD trend. Similar results for synthetic data are provided in SI (Fig. A.2).

3.2. Functional connectivity

Regarding FC simulations, we compared the connectivity reconstructed with $\lambda = 10^{-2}$ and $\lambda = 10^{-1}$ with the ground truth connectivity. The results on the simulations with fully connected networks show an average value of ground truth connectivity equal to 0.95, while the average values of the reconstructed FC with $\lambda = 10^{-2}$ and $\lambda = 10^{-1}$ were 0.66 and 0.56, respectively.

We then performed a paired *t*-test on the difference between ground truth FC and reconstructed FC for each network and each λ value separately. Results highlight that FC with $\lambda = 10^{-2}$ are always closer to the ground truth FC with respect to $\lambda = 10^{-1}$ ($t_{(90)DAN} = 33.4$, $p < 0.001$; $t_{(27)MN} = 13.5$, $p < 0.001$; $t_{(14)VIS} = 21.4$, $p < 0.001$). Regarding the unconnected networks, the ground truth FC was 0.04, and the reconstructed FC with $\lambda = 10^{-2}$ and $\lambda = 10^{-1}$ was 0.19 and 0.39, respectively.

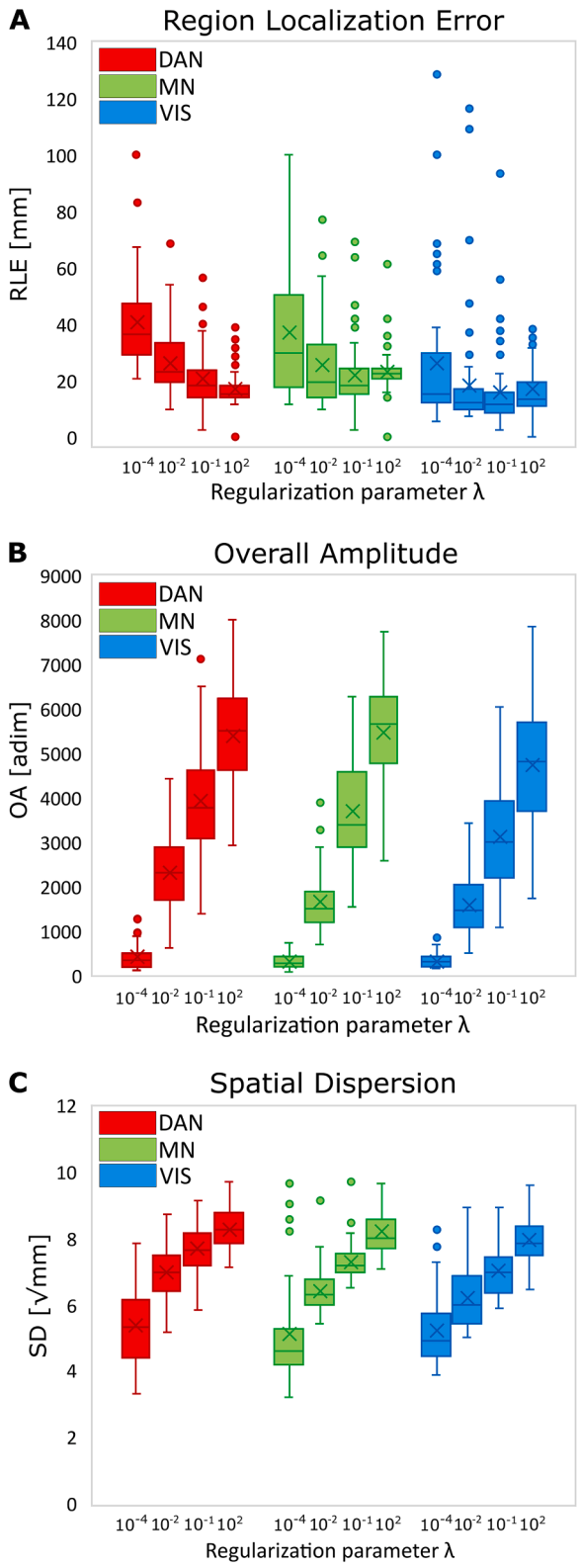

Fig. 4. A. Region Localization Error (RLE) 2.B. Overall Amplitude (OA) and 2. C. Spatial Dispersion (SD) trends at λ values (10^{-4}, 10^{-2}, 10^{-1}, and 10^{2}) for: Visual Network (VIS), in cyan; B) Motor Network (MN) in green; C) Dorsal Attention Network (DAN), in red. Distributions are made by combining the results from every IC of different simulations to take into account different noise values.

Once again, results of the paired *t*-test showed that FC values reconstructed with $\lambda = 10^{-2}$ are higher than the FC with $\lambda = 10^{-1}$ in the DAN and the VIS network ($t_{(90)DAN} = -27.7$, $p < 0.001$; $t_{(14)VIS} = -9.9$, $p < 0.001$). No significant differences were found for MN ($t_{(27)MN} = -0.9$, $p = 0.4$). Difference matrices between ground truth FC values and reconstructed FC values for both fully unconnected and fully connected are given in SI, Fig. A.5 and A.6.

Finally, we reported relative percentage changes (defined in Eq. (10)) in functional connectivity matrices derived from real EEG data in Fig. 7. These results, in combination with the simulated data results that point towards an inflation of functional connectivity values for the highest λ value ($\lambda = 10^{-1}$), speaks for the smallest λ value being able to better recover genuine functional connectivity values.

We computed the BLP (see Materials and Methods Section) from the source space signals in the selected frequency bands. For consistency with the simulated data, we considered only 3 networks (*e.g.*, DAN, VIS, MN) for the following statistical analysis. We found a significant main effect of the factor BAND ($F_{2,60} = 183.88$, $p < 0.001$), as accounted for by higher FC in α as compared to all other bands (post hoc Bonferroni corrected, $p < 0.05$). We also observed a significant main effect of λ ($F_{1,30} = 6.96$, $p < 0.05$), wherein higher FC was associated with a λ value of 10^{-2} compared to a value of 10^{-1}, as depicted in Fig. 8. Furthermore, we did not detect a significant NETWORK effect.

4. Discussion

Gathering information about the brain regions responsible for generating different EEG signals can yield valuable insights into brain function. To estimate the source's location, one must adopt both a model for the source and a model for the head. After selecting these models, an inverse solution can be computed to determine the source's position within the head model. This estimated source is then assumed to represent the actual source. The precision of this source localization method is influenced by several factors, including errors in source modeling, head modeling, measurement locations, and EEG noise (Jatoi et al., 2014).

This study explored the influence of different regularization parameter values on the accuracy of source localization for resting- state EEG activities. We utilized Minimum Norm Estimation on independent components of the brain, while incorporating a realistic head model known as the New York Head. First, we generated synthetic resting-state EEG signals with varying Signal-to-Noise Ratios for three distinct neural networks: the Motor Network, the Visual Network, and the Dorsal Attention Network. The source reconstruction evaluation involved four performance metrics: the Region Localization Error, the source extension, the overall amplitude and the source fragmentation. A summary of the results for these metrics is provided in Table 2. Specifically, the results obtained for SD and OA metrics (Fig. 2A and Fig. 2C) are consistent with the theory behind them (Hauk et al., 2011) and behind MNE. Regarding the spatial dispersion trend, it depends directly on the mathematical definition of MNE (see Eq. (4)). Indeed, when λ increase, the MNE algorithm tends to favor solutions where the energy is minimized; this results in source reconstruction where cortex points have more and more similar source energy, rather than all the energy concentrated on a few points. For this reason, the SD in MNE with higher λ has to be higher. On the other hand, overall amplitude is the normalized sum of reconstructed source amplitude (see Eq. (8)): as already said, when the regularization parameter increases, the maximum of the solution becomes smaller while the total energy remains the same (even if differently distributed throughout the cortex), and that is why OA has to get bigger when λ gets bigger. Regarding the RLE metric, the trend depended on the topography of the considered network and on the lambda values. Indeed, the localization errors were smaller for networks that present very close seeds (as the VIS network), while were higher when networks got more extended (as for the MN and

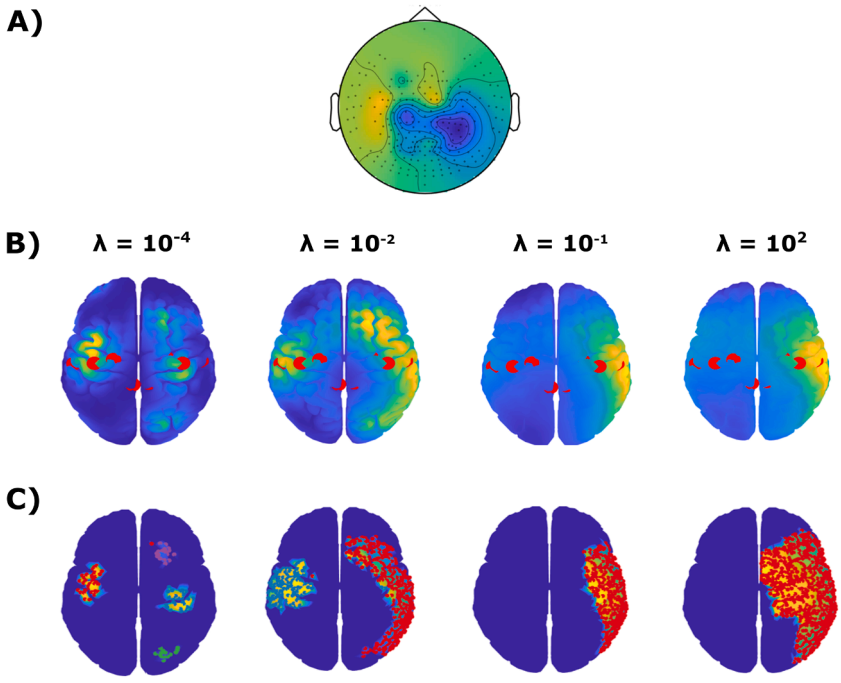

Fig. 5. A) Example of a MN topographic map; B) reconstructed sources at different λ values (10^{-4}, 10^{-2}, 10^{-1}, and 10^{2}). Red points represent ground truth positions of the simulated sources; C) clustering results.

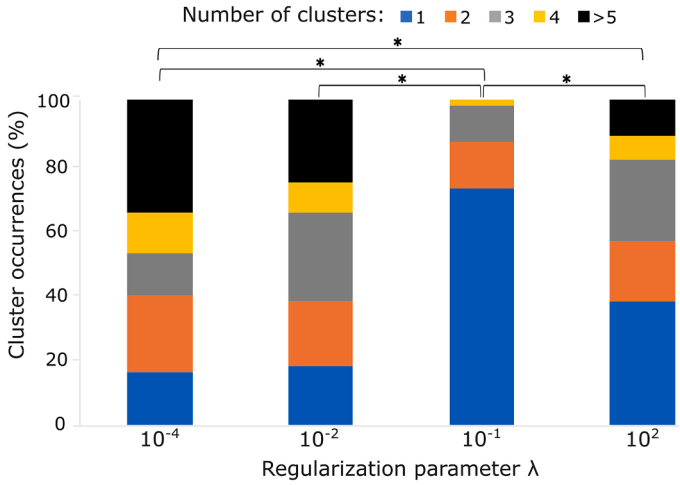

Fig. 6. Percentage of occurrence derived from cluster distribution in real data among λ values equal to 10^{-4}, 10^{-2}, 10^{-1} and 10^{2}. The blue color indicates the presence of one cluster; the orange color, the presence of two clusters; the gray color, the presence of three clusters; the yellow color, the presence of four clusters; the black color, the presence of five clusters.

DAN). This trend occurs since as the brain network spans a larger area, it becomes easier to differentiate between different source points. For instance, when considering VIS seeds, no significant differences were observed among various λ values, primarily due to their proximity, which closely mirrors the spatial resolution of EEG. In contrast, as the network expands across the brain, as seen in MN and especially in DAN, significant variations in RLE with respect to different λ values become evident. Furthermore, contiguous values, such as 10^{-2} and 10^{-1} fail to reveal a significant difference for the RLE metric. Our explanation is that this metric is not sufficiently sensitive to values spaced by only an order of magnitude. By contrast, SD and OA metrics are sensitive to small distances across nodes (*e.g.*, the VIS network) and values, showing significance for all λ values. Then, we performed the clustering analysis with the DBSCAN algorithm on both real and simulated EEG data to evaluate the source fragmentation. Our results suggest that, when λ is equal to 10^{-1}, the solution is minimally fragmented, in contrast to the solutions obtained with 10^{-2} and 10^{-4}, where high numerical instability led to excessive fragmentation.

Finally, we examined the impact of the optimal λ values on the FC estimation in both simulated and real data (a summary of FC results is provided again in Table 2). For the simulated data, we conducted two types of simulations: one where the RSNs were fully connected, and another where they were fully unconnected. In both cases, we compared the reconstructed FC to the ground truth connectivity. Across all RSNs, FC reconstructed with λ equal to 10^{-2} was closer to the ground truth than FC reconstructed with λ equal to 10^{-1} (Fig. A.5 and A.6). It is important to note, however, that the estimated FC was lower than the ground truth in the fully connected case, and higher than the ground truth in the unconnected case. This "smoothing" effect may be attributed to the approximations introduced during source reconstruction, due to the underdetermined nature of the inverse problem. Regarding FC in real data, even if we did not have a ground truth reference for the optimal FC, we can qualitatively see the differences between FC computed with λ equal to 10^{-2} with respect to the traditional value of 10^{-1} found in the literature (Krishnaswamy et al., 2017; Mikulan et al., 2020; Pascarella et al., 2023). For example, in the present work, we can note the effect of the λ value on the FC in the α band. Specifically, we found that, in agreement with previous literature (Samogin et al., 2020), FC was higher in α as compared to all other bands. Another significant effect was found in the value of the λ, which showed higher FC associated with a λ value of 10^{-2} compared to a value of 10^{-1}, as depicted in Fig. 8. Moreover, we did not observe a significant network-related effect that is noteworthy because the strength of FC values remains consistently higher for λ at 10^{-2} regardless of the analyzed resting state networks. Combining this finding with the simulation results, we can infer that the ground truth connectivity in real data is likely higher than our estimates. Indeed, in line with previous fMRI, as well as EEG/MEG, literature (Biswal et al., 1995; Raichle et al., 2001; Fox et al., 2005; Betti et al., 2013; A. 2018; Maddaluno et al., 2024) based on power or amplitude envelope correlation, we expect coherent functional patterns

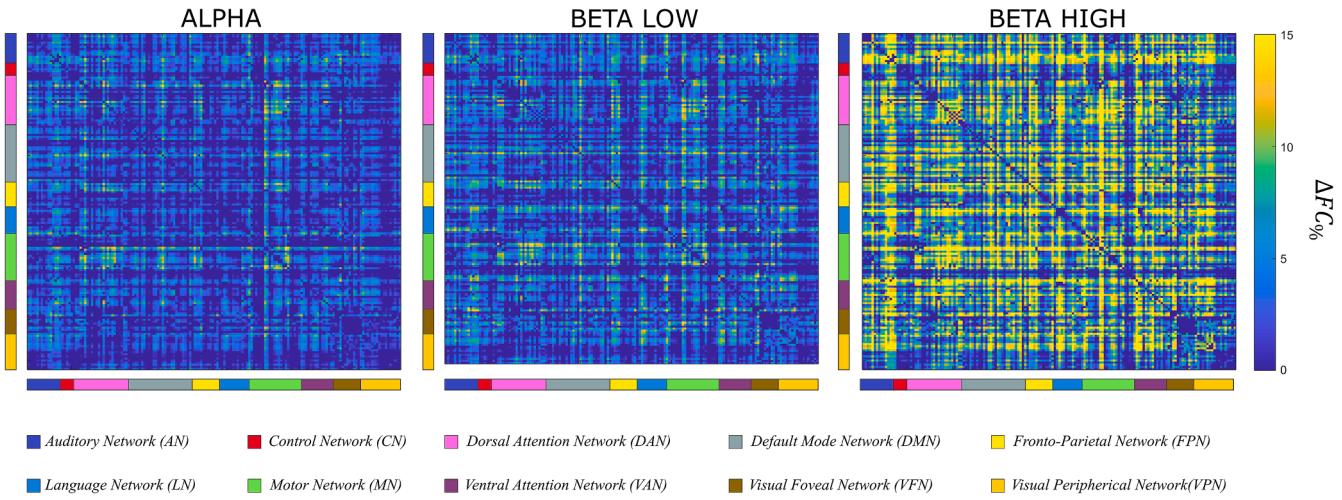

Fig. 7. Percentage relative difference between FC matrices for 164 nodes in 10 RSNs obtained with the two different λ values. Matrices display, for the different frequency bands, the relative percentage changes in FC calculated according to Eq. (10). A positive entry in the matrices indicates an increase in FC for that specific node pair when the source is reconstructed using the smallest λ value.See Fig A.4 in SI for the original matrices from which these relative differences have been calculated.

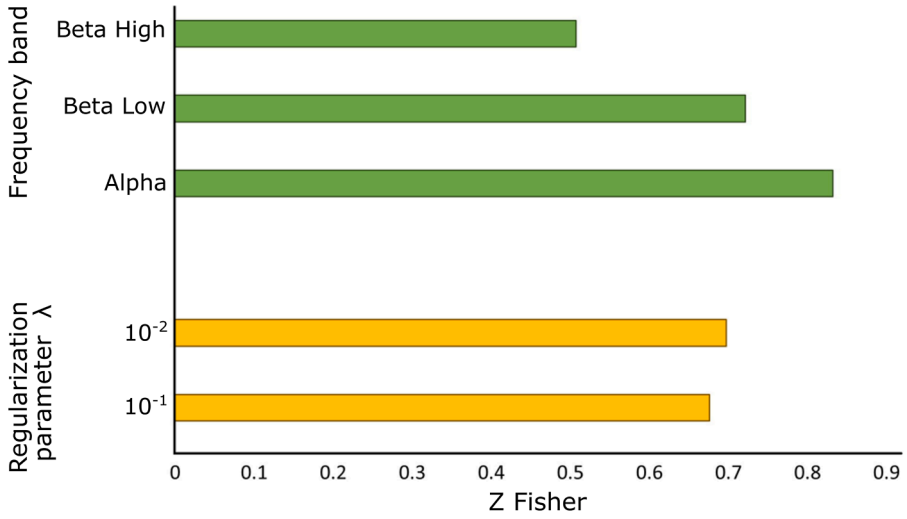

Fig. 8. Representation of Z Fisher values for the significant main effect of frequency band and λ.

Table 2
Summary of the results for all the metrics regarding both source reconstruction and functional connectivity.

		SIMULATED DATA	REAL DATA
SOURCE RECONSTRUCTION	REGION LOCALIZATION ERROR	RLE trend depends on the RSN. 10^{-1} always presents with the lowest value, but there is no significant difference with 10^{-2}	—
	SPATIAL DISPERSION	Neither 10^{-1} nor 10^{-2} are extrema for SD	As for simulated data
	OVERALL AMPLITUDE	Neither 10^{-1} nor 10^{-2} are extrema for OA	As for simulated data
	SOURCE FRAGMENTATION	10^{-1} shows the lowest fragmentation; differences with other λ values are all significant	10^{-1} shows the lowest fragmentation; differences with other λ values are all significant. The trend is even stronger than in simulated data
FUNCTIONAL CONNECTIVITY	FULLY CONNECTED NETWORK	10^{-2} gets closer to ground truth FC than 10^{-1} (both underestimate ground truth FC)	FC ground truth is unknown but combining results from simulated and real data (where 10^{-2} gives back higher FC than 10^{-1}), we can infer that real FC is very strong. This fits with a resting brain model comprised of highly connected RSNs (Raichle et al., 2001)
	FULLY UNCONNECTED NETWORK	10^{-2} gets closer to ground truth FC than 10^{-1} (both overestimate ground truth FC)	—

between signals of nodes of canonical RSNs in the resting brain.

Our finding can be considered highly relevant since there is still an open debate for the selection of the regularization parameter within the context of the current EEG/MEG literature. For instance, in (Samuelsson et al., 2021; Ramírez et al., 2011), the authors compared several source localization techniques, including MNE; they analyzed the impact of λ on source localization, by considering the Localization Error and the Spatial Dispersion parameters, but no analysis was carried out regarding source fragmentation as in our study. Moreover, their study did not investigate functional connectivity. Other works filled this gap by investigating the optimal regularization parameter in MEG functional connectivity (Hincapié et al., 2016; Vallarino et al., 2021, 2023). They found out that the ratio between the regularization parameter for cross-power spectrum estimation and for source localization should be less than 0.5: this finding confirms the trend to use a lower λ value for connectivity than for source localization (Vallarino et al., 2021). In their latest study, the authors expanded this basis by suggesting that the regularization parameter for connectivity estimation should be 1–2 orders of magnitude lower than the optimal value for source localization (Vallarino et al., 2023). Concerning the above-mentioned works (Vallarino et al., 2021, 2023), we considered EEG signals instead of MEG, and we validated our methodological study not only on simulated data but also on real functional connectivity data. In this context, we suggest using λ values equal to 10^{-2} (*i.e.,* $\frac{1}{10^2}$) for connectivity estimation. Regarding source reconstruction, RLE failed to reveal a significant difference between 10^{-1} and 10^{-2}. On the other hand, a significant difference was found for SD and OA between all considered λ values, but no conclusion can be drawn for the best value of regularization parameter. Source fragmentation metric instead showed a clear direction: in real data we found a larger source fragmentation for λ equal to 10^{-2} rather than 10^{-1} (see Fig. 6). Therefore, we still support the conventional practice of using 10^{-1} ($\backsimeq \frac{1}{3^2}$) as a reference for the regularization parameter in source localization.

5. Conclusions

This methodological study underscores the intricate interplay between regularization parameter, neural network topography, and source localization accuracy in high-density EEG for resting-state activity. We support the conventional practice of using 10^{-1} as a reference for the regularization parameter in source reconstruction. Furthermore, we propose using λ equal to 10^{-2} for connectivity estimation. This contribution aims to advance methodological approaches in EEG research and provide valuable guidance for researchers and practitioners striving to enhance source localization's accuracy and reliability in the human brain's complex domain.

CRediT authorship contribution statement

F. Leone: Writing – review & editing, Writing – original draft, Validation, Methodology, Investigation, Formal analysis, Data curation, Conceptualization. **A. Caporali:** Writing – review & editing, Writing – original draft, Investigation, Formal analysis, Conceptualization. **A. Pascarella:** Writing – review & editing, Supervision, Methodology, Conceptualization. **C. Perciballi:** Writing – review & editing, Data curation, Conceptualization. **O. Maddaluno:** Writing – review & editing, Supervision, Methodology, Data curation, Conceptualization. **A. Basti:** Writing – review & editing, Data curation, Conceptualization. **P. Belardinelli:** Writing – review & editing, Supervision, Conceptualization. **L. Marzetti:** Writing – review & editing, Supervision, Methodology, Funding acquisition, Conceptualization. **G. Di Lorenzo:** Writing – review & editing, Supervision, Conceptualization. **V. Betti:** Writing – review & editing, Supervision, Project administration, Methodology, Investigation, Funding acquisition, Data curation, Conceptualization.

Declaration of competing interest

The authors declare that they have no known competing financial interests or personal relationships that could have appeared to influence the work reported in this paper.

Acknowledgements

This project has received funding from the European Research Council (ERC) under the European Union's Horizon 2020 research and innovation programme (HANDmade, grant agreement No 759651) to V. B. V.B. and P.B. are supported by the European Union – NextGeneration EU – Project acronym "CONTACT" Mission 4 component C2, Investment 1.1., CUP B53D23014170006. L.M. is supported by the European Union – NextGeneration EU– Project acronym "NEUROSTAR BTP. Mission 4 component 2, Investment 1.1. CUP D53D23019260001. A.P. is a member of the Gruppo Nazionale Calcolo Scientifico-Istituto Nazionale di Alta Matematica (GNCS-INdAM). AC was supported by the European Union- Next Generation EU, Missione 4, Componente 2, CUP C53D23008470001.

Supplementary materials

Supplementary material associated with this article can be found, in the online version, at doi:10.1016/j.neuroimage.2024.120896.

Data availability

Data will be made available on request.

References

Ahmed, M., Seraj, R., Islam, S.M.S., 2020. The k-means algorithm: a comprehensive survey and performance evaluation. Electronics (Basel) 9, 1295.

Baillet, S., Mosher, J., Leahy, R., 2001. Electromagnetic brain mapping. IEEE Signal Process. Mag. 18, 14–30. https://doi.org/10.1109/79.962275.

Baldassarre, A., Ramsey, L., Hacker, C.L., Callejas, A., Astafiev, S.V., Met- calf, N.V., Zinn, K., Rengachary, J., Snyder, A.Z., Carter, A.R., Shulman, G.L., Corbetta, M., 2014. Large-scale changes in network interactions as a physiological signature of spatial neglect. Brain 137, 3267–3283. https://doi.org/10.1093/brain/awu297. URL10.1093/brain/awu297.

Basti, A., Chella, F., Guidotti, R., Ermolova, M., D'Andrea, A., Sten- roos, M., Romani, G. L., Pizzella, V., Marzetti, L., 2022. Looking through the windows: a study about the dependency of phase- coupling estimates on the data length. J. Neural Eng. 19, 016039. https://doi.org/10.1088/1741-2552/ac542f. URL10.1088/1741-2552/ac542f.

Basti, A., Pizzella, V., Chella, F., Romani, G.L., Nolte, G., Marzetti, L., 2018. Disclosing large-scale directed functional connections in MEG with the multivariate phase slope index. Neuroimage 175, 161–175. https://doi.org/10.1016/j.neuroimage.2018.03.004. URL10.1016/j.neuroimage.2018.03.004.

Betti, V., Della Penna, S., de Pasquale, F., Mantini, D., Marzetti, L., Romani, G., Corbetta, M., 2013. Natural scenes viewing alters the dynamics of functional connectivity in the human brain. Neuron 79, 782–797. https://doi.org/10.1016/j.neuron.2013.06.022. URL10.1016/j.neuron.2013.06.022.

Betti, V., Corbetta, M., de Pasquale, F., Wens, V., Della Penna, S., 2018. Topology of functional connectivity and hub dynamics in the beta band as temporal prior for natural vision in the human brain. J. Neurosci. 38, 3858–3871.

Biswal, B., Zerrin Yetkin, F., Haughton, V.M., Hyde, J.S., 1995. Functional connectivity in the motor cortex of resting human brain using echo-planar mri. Magn. Reson. Med. 34, 537–541.

Brookes, M.J., Woolrich, M., Luckhoo, H., Price, D., Hale, J.R., Stephen- son, M.C., Barnes, G.R., Smith, S.M., Morris, P.G., 2011. Investigating the electrophysiological basis of resting state networks using magnetoen- cephalography. Proc. Natl. Acad. Sci. 108, 16783–16788. https://doi.org/10.1073/pnas.1112685108. URL10.1073/pnas.1112685108.

Calvetti, D., Pascarella, A., Pitolli, F., Somersalo, E., Vantaggi, B., 2019. Brain activity mapping from meg data via a hierarchical bayesian algorithm with automatic depth weighting. Brain Topogr. 32, 363–393.

Chella, F., Marzetti, L., Stenroos, M., Parkkonen, L., Ilmoniemi, R.J., Romani, G.L., Pizzella, V., 2019. The impact of improved MEG–MRI co-registration on MEG connectivity analysis. Neuroimage 197, 354–367. https://doi.org/10.1016/j.neuroimage.2019.04.061. URL10.1016/j.neuroimage.2019.04.061.

Dale, A.M., Liu, A.K., Fischl, B.R., Buckner, R.L., Belliveau, J.W., Lewine, J.D., Halgren, E., 2000. Dynamic statistical parametric mapping: combin- ing fmri and meg for high-resolution imaging of cortical activity. Neuron 26, 55–67.

De Leener, B., Fonov, V.S., Collins, D.L., Callot, V., Stikov, N., Cohen- Adad, J., 2018. Pam50: unbiased multimodal template of the brainstem and spinal cord aligned with the icbm152 space. Neuroimage 165, 170–179.

de Pasquale, F., Della Penna, S., Snyder, A.Z., Lewis, C., Mantini, D., Marzetti, L., Belardinelli, P., Ciancetta, L., Pizzella, V., Romani, G.L., Corbetta, M., 2010. Temporal dynamics of spontaneous meg activity in brain networks. Proc. Natl. Acad. Sci. 107, 6040–6045. https://doi.org/10.1073/pnas.0913863107. URL10.1073/pnas.0913863107.

de Pasquale, F., Della Penna, S., Snyder, A.Z., Marzetti, L., Pizzella, V., Romani, G.L., Corbetta, M., 2012. A cortical core for dynamic inte- gration of functional networks in the resting human brain. Neuron 74, 753–764. https://doi.org/10.1016/j.neuron.2012.03.031. URL10.1016/j.neuron.2012.03.031.

de Pasquale, F., Spadone, S., Betti, V., Corbetta, M., Della Penna, S., 2021. Temporal modes of hub synchronization at rest. Neuroimage 235, 118005. https://doi.org/10.1016/j.neuroimage.2021.118005. URL:10.1016/j.neuroimage.2021.118005.

Doucet, G., Naveau, M., Petit, L., Delcroix, N., Zago, L., Criv- ello, F., Jobard, G., Tzourio-Mazoyer, N., Mazoyer, B., Mel- let, E., Joliot, M., 2011. Brain activity at rest: a multi-scale hierarchical functional organization. J. Neurophysiol. 105, 2753–2763. https://doi.org/10.1152/jn.00895.2010. URL10.1152/jn.00895.2010.

Ester, M., Kriegel, H.P., Sander, J., Xu, X., et al., 1996. A Density-Based Algorithm For Discovering Clusters in Large Spatial Databases With Noise. kdd, pp. 226–231.

Fox, M.D., Snyder, A.Z., Vincent, J.L., Corbetta, M., Van Essen, D.C., Raichle, M.E., 2005. The human brain is intrinsically organized into dynamic, anticorrelated functional networks. Proc. Natl. Acad. Sci. 102, 9673–9678.

Gramfort, A., Luessi, M., Larson, E., Engemann, D.A., Strohmeier, D., Brod- beck, C., Goj, R., Jas, M., Brooks, T., Parkkonen, L., et al., 2013. Meg and eeg data analysis with mne-python. Front. Neurosci. 267.

Grech, R., Cassar, T., Muscat, J., Camilleri, K.P., Fabri, S.G., Zervakis, M., Xanthopoulos, P., Sakkalis, V., Vanrumste, B., 2008. Review on solving the inverse problem in eeg source analysis. J Neuroeng Rehabil 5, 1–33.

Hämäläinen, M., Hari, R., Ilmoniemi, R.J., Knuutila, J., Lounasmaa, O.V., 1993. Magnetoencephalography—Theory, instrumentation, and applications to noninvasive studies of the working human brain. Rev. Mod. Phys. 65 (2), 413.

Hanke, M., Hansen, P.C., 1993. Regularization methods for large-scale prob- lems. Surv. Math. Ind 3, 253–315.

Haufe, S., Nikulin, V.V., Müller, K.R., Nolte, G., 2013. A critical assessment of connectivity measures for EEG data: a simulation study. Neuroimage 64, 120–133. https://doi.org/10.1016/j.neuroimage.2012.09.036. URL10.1016/j.neuroimage.2012.09.036.

Hauk, O., Wakeman, D.G., Henson, R., 2011. Comparison of noise-normalized minimum norm estimates for MEG analysis us- ing multiple resolution metrics. Neuroimage 54, 1966–1974. https://doi.org/10.1016/j.neuroimage.2010.09.053. URL10.1016/j.neuroimage.2010.09.053.

Hincapié, A.S., Kujala, J., Mattout, J., Daligault, S., Delpuech, C., Mery, D., Cosmelli, D., Jerbi, K., 2016. Meg connectivity and power detections with minimum norm estimates require different regularization parameters. Comput. Intell. Neurosci. 2016, 1–11. https://doi.org/10.1155/2016/3979547. URL10.1155/2016/3979547.

Hipp, J.F., Hawellek, D.J., Corbetta, M., Siegel, M., Engel, A.K., 2012. Large-scale cortical correlation structure of spontaneous os- cillatory activity. Nat. Neurosci. 15, 884–890. https://doi.org/10.1038/nn.3101. URL10.1038/nn.3101.

Huang, Y., Parra, L.C., Haufe, S., 2016. The new york head—A precise standardized volume conductor model for EEG source localization and tES targeting. Neuroimage 140, 150–162. https://doi.org/10.1016/j.neuroimage.2015.12.019. URL10.1016/j.neuroimage.2015.12.019.

Hyvarinen, Aapo., 1999. Fast and robust fixed-point algorithms for independent component analysis. IEEE Trans. Neural Networks 10.3, 626–634.

Ilmoniemi, R.J., Sarvas, J., 2019. Brain signals: Physics and Mathematics of MEG and EEG. Mit Press.

Jatoi, M.A., Kamel, N., Malik, A.S., Faye, I., Begum, T., 2014. A survey of methods used for source localization using eeg signals. Biomed. Signal Process. Control 11, 42–52.

Kaipio, J., Somersalo, E., 2007. Statistical inverse prob- lems: discretization, model reduction and inverse crimes. J. Comput. Appl. Math. 198, 493–504. https://doi.org/10.1016/j.cam.2005.09.027. URL10.1016/j.cam.2005.09.027.

Knyazev, G.G., Savostyanov, A.N., Bocharov, A.V., Tamozh- nikov, S.S., Saprigyn, A.E., 2016. Task-positive and task- negative networks and their relation to depression: eeg beam- former analysis. Behav. Brain Res. 306, 160–169. https://doi.org/10.1016/j.bbr.2016.03.033. URL10.1016/j.bbr.2016.03.033.

Krishnaswamy, P., Obregon-Henao, G., Ahveninen, J., Khan, S., Babadi, B., Iglesias, J.E., Hämäläinen, M.S., Purdon, P.L., 2017. Sparsity enables estimation of both subcortical and cortical activ- ity from meg and eeg. Proc. Natl. Acad. Sci. 114. https://doi.org/10.1073/pnas.1705414114. URL10.1073/pnas.1705414114.

Larson-Prior, L.J., Oostenveld, R., Della Penna, S., Michalareas, G., Prior, F., Babajani-Feremi, A., 2013. Adding dynamics to the Human Connectome Project with MEG. Neuroimage 80, 190–201.

Lin, F.H., Witzel, T., Hämäläinen, M.S., Dale, A.M., Belliveau, J.W., Stufflebeam, S.M., 2004. Spectral spatiotemporal imaging of corti- cal oscillations and interactions in the human brain. Neuroimage 23, 582–595. https://doi.org/10.1016/j.neuroimage.2004.04.027. URL10.1016/j.neuroimage.2004.04.027.

Liu, Q., Farahibozorg, S., Porcaro, C., Wenderoth, N., Mantini, D., 2017. Detecting large-scale networks in the human brain us- ing high-density electroencephalography: imaging brain networks with high density eeg. Hum. Brain Mapp. 38, 4631–4643. https://doi.org/10.1002/hbm.23688. URL10.1002/hbm.23688.

Liu, Q., Ganzetti, M., Wenderoth, N., Mantini, D., 2018. Detect- ing large-scale brain networks using eeg: impact of electrode density, head modeling and source localization. Frontiers in Neuroin- formatics 12. https://doi.org/10.3389/fninf.2018.00004. URL10.3389/fninf.2018.00004.

Maddaluno, O., Della Penna, S., Pizzuti, A., Spezialetti, M., Corbetta, M., de Pasquale, F., Betti, V., 2024. Encoding Manual Dexterity through Modulation of Intrinsic α Band Connectivity. J. Neurosci. 44 (20).

Marzetti, L., Della Penna, S., Snyder, A.Z., Pizzella, V., Nolte, G., de Pasquale, F., Romani, G.L., Corbetta, M., 2013. Frequency specific interactions of meg resting state activity within and across brain networks as revealed by the multivariate interaction measure. Neuroimage 79, 172–183.

Mikulan, E., Russo, S., Parmigiani, S., Sarasso, S., Zauli, F.M., Rubino, A., Avanzini, P., Cattani, A., Sorrentino, A., Gibbs, S., et al., 2020. Simulta- neous human intracerebral stimulation and hd-eeg, ground-truth for source localization methods. Sci. Data 7, 127.

Molins, A., Stufflebeam, S., Brown, E., Hämäläinen, M., 2008. Quantification of the benefit from integrating MEG and EEG data in minimum ℓ2-norm estimation. Neuroimage 42, 1069–1077. https://doi.org/10.1016/j.neuroimage.2008.05.064. URL10.1016/j.neuroimage.2008.05.064.

Oostendorp, T.F., Van Oosterom, A., 1989. Source parameter estimation in inhomogeneous volume conductors of arbitrary shape. IEEE Trans. Biomed. Eng. 36, 382–391.

Oostenveld, R., Fries, P., Maris, E., Schoffelen, J.M., 2011. Field- trip: open source software for advanced analysis of meg, eeg, and invasive electrophysiological data. Intell. Neuroscience. https://doi.org/10.1155/2011/156869, 2011URL10.1155/2011/156869.

Pascarella, A., Mikulan, E., Sciacchitano, F., Sarasso, S., Ru- bino, A., Sartori, I., Cardinale, F., Zauli, F., Avanzini, P., No- bili, L., Pigorini, A., Sorrentino, A., 2023. An in–vivo validation of esi methods with focal sources. Neuroimage 277, 120219. https://doi.org/10.1016/j.neuroimage.2023.120219. URL10.1016/j.neuroimage.2023.120219.

Raichle, M.E., MacLeod, A.M., Snyder, A.Z., Powers, W.J., Gusnard, D.A., Shulman, G.L., 2001. A default mode of brain function. Proc. Natl. Acad. Sci. 98, 676–682.

Ramírez, R.R., Kopell, B.H., Butson, C.R., Hiner, B.C., Baillet, S., 2011. Spectral signal space projection algorithm for frequency domain MEG and EEG denoising, whitening, and source imaging. Neuroimage 56 (1), 78–92.

Samogin, J., Marino, M., Porcaro, C., Wenderoth, N., Dupont, P., Swinnen, S.P., Mantini, D., 2020. Frequency-dependent functional connectivity in resting state networks. Hum. Brain Mapp. 41, 5187–5198.

Samuelsson, J.G., Peled, N., Mamashli, F., Ahveninen, J., Hämäläinen, M.S., 2021. Spatial fidelity of MEG/EEG source estimates: a general evaluation approach. Neuroimage 224, 117430. https://doi.org/10.1016/j.neuroimage.2020.117430. URL10.1016/j.neuroimage.2020.117430.

Schoffelen, J., Gross, J., 2009. Source connectivity analysis with meg and eeg. Hum. Brain Mapp. 30, 1857–1865. https://doi.org/10.1002/hbm.20745. URL10.1002/hbm.20745.

Siems, M., Pape, A.A., Hipp, J.F., Siegel, M., 2016. Measur- ing the cortical correlation structure of spontaneous oscilla- tory activity with eeg and meg. Neuroimage 129, 345–355. https://doi.org/10.1016/j.neuroimage.2016.01.055. URL10.1016/j.neuroimage.2016.01.055.

Smith, S.M., Fox, P.T., Miller, K.L., Glahn, D.C., Fox, P.M., Mackay, C.E., Filippini, N., Watkins, K.E., Toro, R., Laird, A.R., et al., 2009. Correspondence of the brain's functional architecture during activation and rest. Proc. Natl. Acad. Sci. 106, 13040–13045.

Smith, S.M., Vidaurre, D., Beckmann, C.F., Glasser, M.F., Jenkinson, M., Miller, K.L., Nichols, T.E., Robinson, E.C., Salimi-Khorshidi, G., Wool- rich, M.W., Barch, D.M., Uğurbil, K., Van Essen, D.C., 2013. Functional connectomics from resting-state fmri. Trends Cogn. Sci. (Regul. Ed.) 17, 666–682. https://doi.org/10.1016/j.tics.2013.09.016. URL10.1016/j.tics.2013.09.016.

Sockeel, S., Schwartz, D., Pélegrini-Issac, M., Benali, H., 2016. Large-scale functional networks identified from resting- state eeg using spatial ica. PLoS One 11, e0146845. https://doi.org/10.1371/journal.pone.0146845. URL10.1371/journal.pone.0146845.

Sommariva, S., Sorrentino, A., Piana, M., Pizzella, V., Marzetti, L., 2017. A comparative study of the robustness of frequency- domain connectivity measures to finite data length. Brain Topogra- phy 32, 675–695. https://doi.org/10.1007/s10548-017-0609-4. URL10.1007/s10548-017-0609-4.

Sorrentino, A., Piana, M., 2017. Inverse modeling for meg/eeg data. Mathematical and Theoretical Neuroscience: Cell. Network and Data Analysis, pp. 239–253.

Tadel, F., Baillet, S., Mosher, J.C., Pantazis, D., Leahy, R.M., 2011. Brain- storm: a user-friendly application for meg/eeg analysis. Computat. Intellig. Neuroscie. 1–13.

Todaro, C., Marzetti, L., Valdés Sosa, P.A., et al., 2019. Mapping brain activity with electrocorticography: resolution properties and robustness of inverse solutions. Brain Topogr. 32, 583–598. https://doi.org/10.1007/s10548-018-0623-1.

Vallarino, E., Sorrentino, A., Piana, M., Sommariva, S., 2021. The role of spectral complexity in connectivity estimation. Axioms 10, 35. https://doi.org/10.3390/axioms10010035. URL10.3390/axioms10010035.

Vallarino, E., Hincapié, A.S., Jerbi, K., Leahy, R.M., Pascarella, A., Sor- rentino, A., Sommariva, S., 2023. Tuning minimum-norm regularization parameters for optimal MEG connectivity estimation. Neuroimage 281, 120356. https://doi.org/10.1016/j.neuroimage.2023.120356. URL10.1016/j.neuroimage.2023.120356.

Wens, V., Marty, B., Mary, A., Bourguignon, M., de Beeck, M.O., Gold- man, S., Bogaert, P.V., Peigneux, P., Tì ege, X.D., 2015. A geometric correction scheme for spatial leakage effects in MEG/EEG seed-based functional connectivity mapping.

Hum. Brain Mapp. 36, 4604–4621. https://doi.org/10.1002/hbm.22943. URL10.1002/hbm.22943.

Winter, W.R., Nunez, P.L., Ding, J., Srinivasan, R., 2007. Comparison of the effect of volume conduction on EEG coherence with the effect of field spread on MEG coherence. Stat. Med. 26 (21), 3946–3957.

Yao, J., Dewald, J.P., 2005. Evaluation of different cortical source localization methods using simulated and experimental EEG data. Neuroimage 25, 369–382. https://doi.org/10.1016/j.neuroimage.2004.11.036. URL10.1016/j.neuroimage.2004.11.036.